An improved $k - \omega$ turbulence model applied to recirculating flows

Jonas Bredberg [*], Shia-Hui Peng [1], Lars Davidson

Department of Thermo and Fluid Dynamics, Chalmers University of Technology, S-412 96 Gothenburg, Sweden

Abstract

In this paper an improved $k - \omega$ turbulence model is proposed, which brings the asymptotic boundary value for ω into accord with direct numerical simulation (DNS) data. In the new ω-equation both a turbulent and a viscous cross-diffusion term are included, justified by an analogy to the Yap-correction and the pressure-diffusion process, respectively. The importance of cross-diffusion terms in removing the freestream sensitivity with respect to ω for free shear flows is shown. The performance of the model is evaluated and compared with DNS and with other turbulence models in a channel flow, a backward-facing step flow and a rib-roughened channel flow with heat transfer. The model requires neither wall-function nor wall-distance information and is fully integrable over the near-wall region.

1. Introduction

The Reynolds averaging of the Navier–Stokes equations results in the Reynolds stress tensor, $\tau_{ij} = \overline{u_i u_j}$, in the momentum equations and the heat-flux vector, $\overline{u_i \theta}$, in the thermal energy equation. These unknowns need to be modelled in order to close the equation system. In the framework of eddy-viscosity models (EVMs) the Reynolds stress tensor is modelled with the Boussinesq hypothesis, which assumes an alignment between the τ_{ij} and the mean flow deformation, via an eddy-viscosity, v_t. The turbulent stresses/heat fluxes are thus modelled in analogy to their molecular counterparts. The eddy-viscosity, v_t, is modelled using a velocity scale, u, and a length scale, l, as

$$v_t \sim ul \tag{1}$$

In two-equation EVMs these quantities are obtained using two turbulent transport equations, where the turbulent kinetic energy, k, is normally used for the

velocity scale, $u \sim \sqrt{k}$, while the length scale is modelled with k and an additional turbulent quantity. In the $k - \varepsilon$ models (see e.g. Jones and Launder (1972)), the length scale is approximated in terms of k and its dissipation rate, ε, as $l \sim k^{3/2}/\varepsilon$, while in the $k - \omega$ models (see e.g. Wilcox (1998)), the reciprocal of turbulent time scale, ω, is used, hence $l \sim \sqrt{k}/\omega$. There exists several other types of two-equation EVMs such as the $k - \tau$ model by Speziale et al. (1992) which solves for the turbulent time scale, and the $k - v_t$ model, by Peng and Davidson (2000), which solves directly for the turbulent viscosity itself.

Since the dissipation rate of turbulent kinetic energy, ε, appears naturally in the exact equation for the turbulent kinetic energy, it is the obvious choice for the second turbulent quantity in the formulation for v_t. However both physically and numerically, ε may not be the optimum choice. Analyses based on direct numerical simulation (DNS) data show that ε is non-zero and finite at walls, which is difficult to specify. A remedy to this problem has been to solve for the reduced dissipation rate, $\tilde{\varepsilon}$, and include an additional term in the k-equation (see e.g. Launder and Sharma (1974)). Another possible solution to this deficiency is to solve for an alternative quantity to ε. For example the $k - \tau$ and $k - v_t$ models have well-posed wall boundary condition with $\tau = 0$, and $v_t = 0$, respectively. In the $k - \omega$ model, the wall

---

[*] Corresponding author. Present address: Volvo Aero Corporation, Military Engines Division, S-461 81 Trollhättan, Sweden.

E-mail address: bredberg@tfd.chalmers.se (J. Bredberg).

[1] Present address: Computational Aerodynamics, Aeronautics Division (FFA), Swedish Defence Research Agency (FOI), S-172 90 Stockholm, Sweden.

Nomenclature

A	cross-section area
C	turbulence model constant with various subscripts
C_f	skin friction coefficient
D_h	hydraulic diameter
e	rib size
f_μ	damping function
h	step height
H	channel height
k	turbulent kinetic energy
l	turbulent length scale
$\dot{m}$	mass flow
Nu	Nusselt number
P	distance between two consecutive ribs (pitch)
P	mean pressure
p	pressure fluctuation
$P_k, P_\varepsilon, P_\omega$	production terms
Pr	Prandtl number, $Pr = 0.71$ for air
Pr_t	turbulent Prandtl number
Re	Reynolds number, UH/v
R_t	turbulent Reynolds number, v_t/v or $k/(\omega v)$
t	time
U_i	mean velocities
u_i	velocity fluctuations
$\overline{u_i u_j}$	Reynolds stresses
x	streamwise distance
y	wall normal distance

Greeks

δ'	free shear layer spreading rate, $\delta' \sim d\delta/dx$, according to Wilcox (1998)
ε	dissipation rate of k
κ	van Karman constant, $\kappa = 0.41$
v	kinematic viscosity
v_t	turbulent eddy-viscosity
ρ	density
ω	specific dissipation rate
Π	pressure-diffusion term
Ψ	destruction term
$\sigma_k, \sigma_\varepsilon, \sigma_\omega$	turbulence model constant
τ	turbulent time scale
τ_w	wall shear, ρu_τ^2
Θ	mean temperature
θ	temperature fluctuations

Superscripts

$+$	normalised variables using wall parameters
v	viscous part
T	turbulent part

Subscripts

b	bulk value
r	re-attachment value
w	wall value
τ	value based on the friction velocity, $u_\tau = \sqrt{\tau_w/\rho}$
∞	freestream value

boundary condition for ω is $\omega_w \sim y^{-2}$, which has been shown to have a numerically stabilising effect. In a study by Huang and Bradshaw (1995), it was concluded that the optimum choice for the length scale determining equation is the specific dissipation rate, $\omega = \varepsilon/k$, based on the performance of EVMs for flows with adverse pressure gradient.

In this work, the $k - \omega$ model is further improved by reviewing the modelling of the ω-equation. Speziale et al. (1992) showed that, through a transformation from the ε-equation, the appropriate wall boundary condition for ω is $2v/y^2$, which is indeed consistent with DNS data for channel flow. It is argued that the inclusion of a viscous cross-diffusion term not only enables the correct asymptotical wall boundary condition for ω, but also is a reasonable approximation to the pressure-diffusion term in the ω-equation.

In addition a turbulent cross-diffusion term is included, which is argued from the transformation of the ε-equation and the two-scale direct interaction approximation (TSDIA) of Yoshizawa (1987). It is shown that the turbulent cross-diffusion term may be an analogy to the Yap correction (Yap, 1987), which im-

proves the heat transfer prediction for recirculating flows.

It is demonstrated that a major weakness of the Wilcox $k - \omega$ models; the freestream sensitivity with respect to ω, can be greatly relaxed through a careful calibration of the cross-diffusion terms in the ω-equation.

In the present work, through the addition of the viscous cross-diffusion term, the number of damping terms is reduced. The model uses only one wall-distance free damping function, with dependency upon the turbulent Reynolds number, R_t. This simplifies the computation of flows in complex geometries, avoiding any ambiguities with the proper wall-distance in corners.

The new $k - \omega$ turbulence model is validated for fully developed turbulent channel flow in comparison with DNS data. Improved predictions, as compared with the $k - \varepsilon - v^2 - f$ model (Lien and Kalitzin, 2001), a $k - \varepsilon$ model (Abe et al., 1994) and a $k - \omega$ model (Wilcox, 1993), are presented for a backward-facing step (BFS) flow and a rib-roughened channel flow with heat transfer.

2. Model formulation

2.1. Governing equations

The governing equations for an incompressible flow are the continuity equation, the momentum equations and the temperature equation. These are respectively

$$\frac{\partial U_i}{\partial x_i} = 0 \tag{2}$$

$$\frac{\mathrm{D}U_i}{\mathrm{D}t} = -\frac{1}{\rho}\frac{\partial P}{\partial x_i} + \frac{\partial}{\partial x_j}\left(v\frac{\partial U_i}{\partial x_j} - \overline{u_i u_j}\right) \tag{3}$$

$$\frac{\mathrm{D}\Theta}{\mathrm{D}t} = \frac{\partial}{\partial x_i}\left(\frac{v}{Pr}\frac{\partial \Theta}{\partial x_i} - \overline{u_i\theta}\right) \tag{4}$$

As discussed above this equation system is not closed due to the Reynolds stress tensor, $\overline{u_i u_j}$, in the momentum equations and the heat flux vector, $\overline{u_i\theta}$, in the temperature equation. In an EVM the Reynolds stress tensor is modelled through the Boussinesq hypothesis

$$-\overline{u_i u_j} = v_t\left(\frac{\partial U_i}{\partial x_j} + \frac{\partial U_j}{\partial x_i}\right) - \frac{2}{3}k\delta_{ij} \tag{5}$$

In a low-Reynolds number (LRN) turbulence model the eddy-viscosity, v_t, is modelled as

$$v_t = C_\mu f_\mu \frac{k^2}{\varepsilon} \quad \text{or} \quad v_t = C_\mu f_\mu \frac{k}{\omega} \tag{6}$$

where C_μ is a constant and f_μ is a damping function. The turbulent heat-flux vector is modelled as

$$-\overline{u_i\theta} = \frac{v_t}{Pr_t}\frac{\partial \Theta}{\partial x_i} \tag{7}$$

where the turbulent Prandtl number, Pr_t, is either set as a constant or computed from an algebraic relation as proposed by Kays and Crawford (1993)

$$Pr_t = \frac{1}{0.5882 + 0.228R_t - 0.0441R_t^2[1 - \exp(-5.165/R_t)]} \tag{8}$$

where R_t is the turbulent Reynolds number with $R_t = v_t/v$.

2.2. The $k - \varepsilon$ model

The exact equations for the turbulent kinetic energy and its dissipation rate are

$$\frac{\mathrm{D}k}{\mathrm{D}t} = P_k - \varepsilon + \Pi_k + D_k^{\mathrm{T}} + \frac{\partial}{\partial x_j}\left(v\frac{\partial k}{\partial x_j}\right) \tag{9}$$

$$\frac{\mathrm{D}\varepsilon}{\mathrm{D}t} = P_\varepsilon - \Phi_\varepsilon + \Pi_\varepsilon + D_\varepsilon^{\mathrm{T}} + \frac{\partial}{\partial x_j}\left(v\frac{\partial \varepsilon}{\partial x_j}\right) \tag{10}$$

where P_k and P_ε are the production terms, ε and Φ_ε are the destruction terms, D_k^{T} and $D_\varepsilon^{\mathrm{T}}$ are the turbulent dif-

fusion term, and the last terms in Eqs. (9) and (10) are the viscous diffusion terms.

For the k-equation the Boussinesq hypothesis is incorporated into the production term, viz

$$P_k = -\overline{u_i u_j}\frac{\partial U_i}{\partial x_j} \stackrel{\mathrm{Eq.(5)}}{=} v_t\left(\frac{\partial U_i}{\partial x_j} + \frac{\partial U_j}{\partial x_i}\right)\frac{\partial U_i}{\partial x_j} \tag{11}$$

and the standard gradient diffusion hypothesis (SGDH) is used for the diffusion terms

$$\Pi_k + D_k^{\mathrm{T}} = -\frac{\partial}{\partial x_j}\left(\frac{\overline{u_j p}}{\rho} + \overline{u_j u_i u_i}\right) \approx \frac{\partial}{\partial x_j}\left(\frac{v_t}{\sigma_k}\frac{\partial k}{\partial x_j}\right) \tag{12}$$

The dissipation rate, ε, in the k-equation is computed from its own transport equation. The modelled k-equation reads

$$\frac{\mathrm{D}k}{\mathrm{D}t} = P_k - \varepsilon + \frac{\partial}{\partial x_j}\left[\left(v + \frac{v_t}{\sigma_k}\frac{\partial k}{\partial x_j}\right)\right] \tag{13}$$

The transport equation for the dissipation rate is modelled similarly to the k-equation as

$$\frac{\mathrm{D}\varepsilon}{\mathrm{D}t} = C_{\varepsilon 1}\frac{\varepsilon}{k}P_k - C_{\varepsilon 2}\frac{\varepsilon^2}{k} + \frac{\partial}{\partial x_j}\left[\left(v + \frac{v_t}{\sigma_\varepsilon}\frac{\partial \varepsilon}{\partial x_j}\right)\right] \tag{14}$$

with the following constants, as suggested by Launder and Spalding (1974)

$$C_{\varepsilon 1} = 1.44, \quad C_{\varepsilon 2} = 1.92, \quad \sigma_k = 1.0, \quad \sigma_\varepsilon = 1.3 \tag{15}$$

For LRN modified models a damping function, f_2, is often multiplied to the constant $C_{\varepsilon 2}$.

2.3. Transformation from a $k - \omega$-model to a $k - \omega$-model

The specific dissipation rate of turbulent kinetic energy, ω, is defined as

$$\omega \equiv \frac{\varepsilon}{C_k k} \tag{16}$$

Consequently the ω-equation may be constructed from the k- and ε-equations. That is

$$\frac{\mathrm{D}\omega}{\mathrm{D}t} = \frac{\mathrm{D}}{\mathrm{D}t}\left(\frac{\varepsilon}{C_k k}\right) = \frac{1}{C_k k}\frac{\mathrm{D}\varepsilon}{\mathrm{D}t} - \frac{\omega}{k}\frac{\mathrm{D}k}{\mathrm{D}t} \tag{17}$$

Inserting the exact equations for k (Eq. (9)) and ε (Eq. (10)) in Eq. (17) yields

$$\frac{\mathrm{D}\omega}{\mathrm{D}t} = \underbrace{\left[\frac{1}{C_k k}P_\varepsilon - \frac{\omega}{k}P_k\right]}_{\text{Production, }P_\omega} - \underbrace{\left[\frac{1}{C_k k}\Phi_\varepsilon - \frac{\omega}{k}\varepsilon\right]}_{\text{Destruction, }\Phi_\omega}$$

$$+ \underbrace{\left[\frac{1}{C_k k}\Pi_\varepsilon - \frac{\omega}{k}\Pi_k\right]}_{\text{Pressure diffusion, }\Pi_\omega} + \underbrace{\left[\frac{1}{C_k k}D_\varepsilon^{\mathrm{T}} - \frac{\omega}{k}D_k^{\mathrm{T}}\right]}_{\text{Turbulent diffusion, }D_\omega^{\mathrm{T}}}$$

$$+ \underbrace{\left[\frac{1}{C_k k}v\frac{\partial^2 \varepsilon}{\partial x_j^2} - \frac{\omega}{k}v\frac{\partial^2 k}{\partial x_j^2}\right]}_{\text{Viscous diffusion, }D_\omega^v} \tag{18}$$

Using the standard $k - \varepsilon$-model the resulting modelled ω-equation becomes

$$\frac{D\omega}{Dt} = P_\omega - \Phi_\omega + \Pi_\omega + D_\omega^T + D_\omega^v \qquad (19)$$

where

$$P_\omega = \left(\frac{1}{C_k k} C_{\varepsilon 1} \frac{\varepsilon}{k} - \frac{\omega}{k} \right) P_k = (C_{\varepsilon 1} - 1) \frac{\omega}{k} P_k$$

$$\Phi_\omega = \frac{1}{C_k k} C_{\varepsilon 2} \frac{\varepsilon^2}{k} - \frac{\omega}{k} C_k \omega k = (C_{\varepsilon 2} - 1) C_k \omega^2$$

$$\Pi_\omega = 0$$

$$D_\omega^v = \frac{1}{C_k k} v \frac{\partial^2 \varepsilon}{\partial x_j^2} - \frac{\omega}{k} v \frac{\partial^2 k}{\partial x_j^2} = \frac{2v}{k} \frac{\partial k}{\partial x_j} \frac{\partial \omega}{\partial x_j} + v \frac{\partial^2 \omega}{\partial x_j^2}$$

$$D_\omega^T = \frac{1}{C_k k} \frac{\partial}{\partial x_j} \left(\frac{v_t}{\sigma_\varepsilon} \frac{\partial \varepsilon}{\partial x_j} \right) - \frac{\omega}{k} \frac{\partial}{\partial x_j} \left(\frac{v_t}{\sigma_k} \frac{\partial k}{\partial x_j} \right)$$

$$= \frac{v_t}{k} \left(\frac{1}{\sigma_\varepsilon} + \frac{1}{\sigma_k} \right) \frac{\partial k}{\partial x_j} \frac{\partial \omega}{\partial x_j} + v_t \frac{\omega}{k} \left(\frac{1}{\sigma_\varepsilon} - \frac{1}{\sigma_k} \right) \frac{\partial^2 k}{\partial x_j^2} + v_t$$

$$\times \frac{\omega}{k^2} \left(\frac{1}{\sigma_\varepsilon} - \frac{1}{\sigma_k} \right) \left(\frac{\partial k}{\partial x_j} \right)^2 + \frac{\partial}{\partial x_j} \left(\frac{v_t}{\sigma_\varepsilon} \frac{\partial \omega}{\partial x_j} \right)$$

The main difference between this and the ω-equation in the Wilcox model (1988, 1993) is the cross-diffusion terms, i.e. the terms proportional to $\partial k/\partial x_j \partial \omega/\partial x_j$.

A well known weakness of the Wilcox $k - \omega$ models is the freestream sensitivity with respect to ω. This is particularly true for free shear flows, for which it is possible to predict almost arbitrary result through different, although reasonable, freestream values of ω. Menter (1991) proposed a remedy to this problem by introducing a turbulent cross-diffusion term, $v_t/k \partial k/\partial x_j \partial \omega/\partial x_j$, in the ω-equation. Recently proposed $k - \omega$ models by Menter (1994), Peng et al. (1997), Wilcox (1998) and Kok (2000) have all included such a term.

In Fig. 1, the predicted spreading rates using the present model, which includes both a viscous and a turbulent cross-diffusion term, is compared with the standard $k - \omega$ model, Wilcox (1993) and the modified $k - \omega$ model by Peng et al. (1997) (PDH). The $k - \varepsilon$ model by Abe et al. (1994) (AKN) is used as a reference model. The results are normalised with the predicted spreading rate, $\delta' = d\delta/dx$, using a $\omega_{\infty,\text{ref}}$ equivalent to setting the eddy-viscosity to a small value, 10^{-7}.

Here it is re-confirmed that the accuracy of the Wilcox model is severely affected by the chosen ω_∞. The addition of cross-diffusion terms, however significantly reduces the $k - \omega$ models freestream sensitivity with respect to ω. The present model predicts a behaviour similar to the $k - \varepsilon$ model, while the PDH-model, without a viscous cross-diffusion term, yields inaccurate results only for large values of ω_∞.
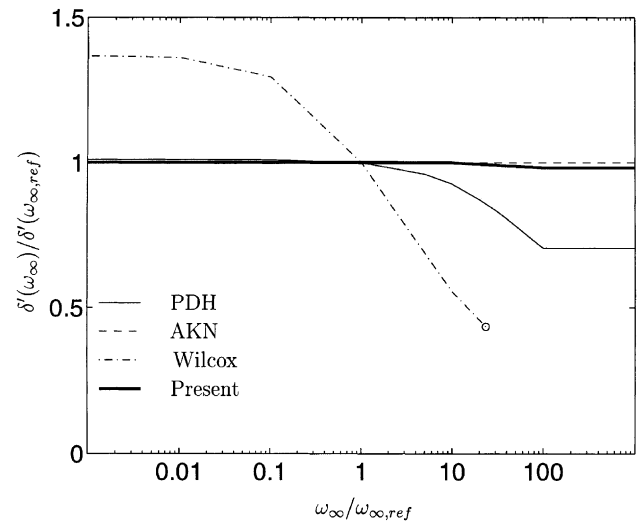
(a) Mixing layer
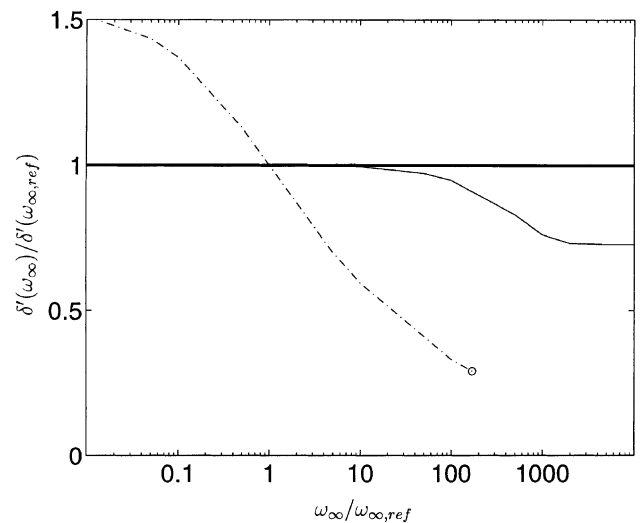
(b) Round jet

Fig. 1. Spreading rates, free shear flows.

In addition to the improvements for free shear flows, Speziale et al. (1992) showed that the inclusion of the viscous cross-diffusion term is essential for wall bounded flows. The near-wall balance of the ω-equation is

$$-(C_{\varepsilon 2} - 1) C_k \omega^2 + \frac{2v}{k} \frac{\partial k}{\partial y} \frac{\partial \omega}{\partial y} + v \frac{\partial^2 \omega}{\partial y^2} = 0 \qquad (20)$$

Applying a LRN turbulence model with a damping function, f_2, to the coefficient $C_{\varepsilon 2}$, the asymptotic relation for ω becomes, with $f_2 C_{\varepsilon 2} \to 0$ and $k \sim y^2$ as $y \to 0$

$$\omega \to \frac{2v}{C_k y^2} \qquad (21)$$

With the above definition of ω, Eq. (16), this relation is consistent with DNS-data (Mansour et al., 1988) for the dissipation rate

$$\varepsilon_{\mathrm{w}} = v \left. \frac{\partial^2 k}{\partial y^2} \right|_{y=0} \approx 2v \frac{k}{y^2} \tag{22}$$

The above results clearly demonstrates the importance of including both a viscous and a turbulent cross-diffusion term in the ω-equation. Contrary to the present model, the non cross-diffusion modified Wilcox $k - \omega$ models is neither able to capture a correct free-stream behaviour, nor being compatible with near-wall DNS data.

2.4. Modelling the k- and ω-equations

2.4.1. The damping function, f_μ

The inclusion of damping functions is a result of accounting for viscous and wall-damping effects. Through proper treatment of the exact terms, such effects may be partly represented by the modelled terms without using damping functions. In the present model the viscous cross-diffusion term plays such a role in the viscous sub-layer by reducing ω.

To yield correct near-wall asymptotic behaviour for the turbulent shear stress a damping function, f_μ, is introduced for v_t, Eq. (6). In accordance with Wilcox (1993), the damping function should in the limit of $R_t \to 0$ comply with

$$C_{\omega 1} C_\mu f_\mu < C_{\omega 2}$$
$$\frac{C_k}{C_\mu f_\mu} \to 1 \tag{23}$$

These conditions necessitates that $f_\mu \to 0.09$, as $R_t \to 0$. In addition the damping function should approach unity for fully developed turbulent flows, hence $f_\mu \to 1$, as $R_t \to \infty$.

Following Hanjalic and Launder (1976), the fluctuating quantities in the vicinity of a wall, using Taylor expansion series is

$$\begin{aligned} u &= a_1 y + b_1 y^2 + \cdots \\ v &= b_2 y^2 + \cdots \\ w &= a_3 y + b_3 y^2 + \cdots \\ p &= a_4 + b_4 y + \cdots \end{aligned} \tag{24}$$

By the definition of k and ε the asymptotic relations for them are $k \sim y^2$ and $\varepsilon \sim y^0$, respectively. Consequently, the specific dissipation rate varies as $\omega \sim y^{-2}$, when $y \to 0$. Thus the damping function should vary as y^{-1} to impose a correct near-wall behaviour for the turbulent shear stress.

It is numerically convenient to avoid any wall-distance dependencies in a model when applied to flows in complex geometries. A commonly used parameter for damping function in devising wall-distance free damping functions is the turbulent Reynolds number, defined in a $k - \omega$ model as $R_t = k/(\omega v)$.

The damping function in the present model is devised as

$$f_\mu = 0.09 + \left(0.91 + \frac{1}{R_t^3}\right)\left[1 - \exp\left\{-\left(\frac{R_t}{25}\right)^{2.75}\right\}\right] \tag{25}$$

which has been optimised numerically using DNS data for channel flow. Note that $R_t^{-0.25} \sim y^{-1}$.

2.4.2. Modelling the pressure-diffusion term

The modelling of the pressure-diffusion term has historically been rather rudimentary, mainly due to the difficulties of measuring the near-wall velocity–pressure correlations. In the $k - \varepsilon$ model, the pressure-diffusion term has either been neglected or modelled together with the triple velocity-correlation term through the SGDH, Eq. (12). The values of σ_k and σ_ε have traditionally been tuned to give accurate results in the logarithmic region, with less attention paid to their near-wall accuracy.

In the DNS analyses by Mansour et al. (1988) and Rodi and Mansour (1993), it was shown that the turbulent diffusion process, $(\Pi_k + D_k^{\mathrm{T}})$, close to the wall does not decrease as rapidly as a SGDH-type turbulent diffusion model, would predict. A remedy to this has been to allow near-wall σ_k and σ_ε to vary, see e.g. the Hwang and Lin $k - \varepsilon$ model (1998).

Furthermore the DNS data indicates that even though the pressure-diffusion process has generally little influence, it becomes significant for the balance of the equations in the viscous sub-layer, where the dissipation is balanced by both the viscous- and pressure-diffusion terms.

The pressure-diffusion term in the exact ω-equation can be obtained by a transformation of the exact pressure-diffusion terms in the k- and ε-equations as

$$\begin{aligned} \Pi_\omega &= \frac{1}{C_k k} \Pi_\varepsilon - \frac{\omega}{k} \Pi_k \\ &= -\frac{1}{C_k k} \frac{2v}{\rho} \frac{\partial}{\partial x_j}\left(\overline{\frac{\partial p}{\partial x_k} \frac{\partial u_j}{\partial x_k}}\right) + \frac{\omega}{k} \frac{1}{\rho} \frac{\partial}{\partial x_j}\left(\overline{pu_j}\right) \end{aligned} \tag{26}$$

Analysis of the asymptotic near-wall properties of Eq. (26) suggests that

$$\begin{aligned} -\underbrace{\frac{1}{C_k k} \frac{2v}{\rho} \frac{\partial}{\partial x_j}\left(\overline{\frac{\partial p}{\partial x_k} \frac{\partial u_j}{\partial x_k}}\right)}_{\Pi_\varepsilon} &\to y^{-2} \\ +\underbrace{\frac{\omega}{k} \frac{1}{\rho} \frac{\partial}{\partial x_j}\left(\overline{pu_j}\right)}_{\Pi_k} &\to y^{-3} \end{aligned} \tag{27}$$

In the near-wall region, the contribution of the pressure-diffusion of the k-equation is thus more important than that of the pressure-diffusion of the ε-equation. Based on analysis of DNS data, Kawamura (1991) proposed a cross-diffusion type model for Π_k,

which was used in e.g. the Hwang and Lin $k - \varepsilon$ turbulence model. It reads

$$\Pi_k = C_\Pi v \frac{\partial}{\partial x_j} \left(\frac{k}{\varepsilon} \frac{\partial \varepsilon}{\partial x_j} \right) \tag{28}$$

Transforming Eq. (28) in terms of k and ω gives

$$\Pi_k = C_\Pi v \frac{\partial}{\partial x_j} \left(\frac{1}{\omega} \frac{\partial k\omega}{\partial x_j} \right)$$

$$= C_\Pi v \left[\frac{1}{\omega} \frac{\partial k}{\partial x_j} \frac{\partial \omega}{\partial x_j} + \frac{\partial^2 k}{\partial x_j^2} - \frac{k}{\omega^2} \left(\frac{\partial \omega}{\partial x_j} \right)^2 + \frac{k}{\omega} \frac{\partial^2 \omega}{\partial x_j^2} \right] \tag{29}$$

with $k \sim y^2$ and $\omega \sim y^{-2}$, a near-wall analysis shows that the four terms on the right-hand-side balance each other to the first order, yielding an asymptotic dependence for Π_k as y. However when transformed, via Eq. (26), these terms would impose an inaccurate near-wall behaviour for the ω-equation as y^{-3}. By including only the cross-diffusion term the near-wall dependency of ω-equation is maintained, and hence the pressure-diffusion is modelled as

$$\Pi_\omega = -\frac{\omega}{k} \Pi_k = -C_\Pi \frac{v}{k} \frac{\partial k}{\partial x_j} \frac{\partial \omega}{\partial x_j} \tag{30}$$

with the near-wall balance for ω given as (cf. Eq. (20))

$$-(C_{\varepsilon 2} - 1)C_k \omega^2 + (2 - C_\Pi) \frac{v}{k} \frac{\partial k}{\partial x_j} \frac{\partial \omega}{\partial x_j} + v \frac{\partial^2 \omega}{\partial x_j^2} = 0 \tag{31}$$

In Eq. (20), the near-wall ω could only be fulfilled through the inclusion of a damping function, f_2. With the addition of the pressure-diffusion model this can however be avoided through the usage of appropriate coefficients. The ratio of $C_{\omega 2} \equiv (C_{\varepsilon 2} - 1)C_k$ and C_k can be established in decaying turbulence where experimental observation indicates that (Townsend, 1976)

$$k \sim t^{-n}, \quad n = 1.25 \pm 0.06 \tag{32}$$

For a $k - \omega$ model, Wilcox (1998) shows that $n = C_k / C_{\omega 2}$. With $C_k = 0.09$ the range for $C_{\omega 2}$ is: $0.069 < C_{\omega 2} < 0.076$. Using $C_{\omega 2} = 0.072$, the correct asymptotic relation for ω, given by Eq. (21), is achieved provided that, $C_\Pi = 0.9$.

2.4.3. Modelling the turbulent cross-diffusion term

For non-equilibrium flows, the $k - \varepsilon$ model often predicts a too large turbulent length-scale, leading to an overprediction of v_t and consequently the heat transfer. Yap (1987) was able to improve the result through an additional term in the ε-equation, i.e. the Yap-correction, which reduces the length-scale by increasing the dissipation. It can be argued that the inclusion of a turbulent cross-diffusion term may play a similar role.

Using TSDIA, Yoshizawa (1987) derived a sophisticated model for the turbulent diffusion process, which introduce cross-diffusion terms, similar to those given

above, Eq. (19). The TSDIA produces cross-diffusion terms in both the k- and ε-equations, although Yoshizawa (1987) pointed out that the inclusion of such terms in the k-equation would not render an improved performance compared to the standard k-equation. For the ε-equation, however, Yoon and Chung (1995) concluded that a cross-diffusion term may significant improve the model behaviour for non-equilibrium flows.

In the $k - \varepsilon$ model of Yoon and Chung (1995) the cross-diffusion term in the ε-equation takes the form

$$D_\varepsilon^{CD} = C_\varepsilon v_t \frac{\partial k}{\partial x_j} \frac{\partial (\varepsilon/k)}{\partial x_j} \tag{33}$$

This term would, similarly to the Yap-correction, increase the dissipation if, $C_\varepsilon < 0$, since in the near-wall region, $\partial(\varepsilon/k)/\partial y < 0$ and $\partial k/\partial y > 0$. Transforming Eq. (33) to the ω-equation yields, with the definition of ω as in Eq. (16)

$$D_\omega^{CD} = \frac{1}{C_k k} D_\varepsilon^{CD} = C_\varepsilon \frac{v_t}{k} \frac{\partial k}{\partial x_j} \frac{\partial \omega}{\partial x_j} \tag{34}$$

Thus the combination of the Yap-correction term, Eq. (34) and the turbulent cross-diffusion term from the transformation of the ε-equation, Eq. (19) results in the following term in the ω-equation

$$\frac{v_t}{k} \underbrace{\left(\frac{1}{\sigma_\omega} + \frac{1}{\sigma_k} + C_\varepsilon \right)}_{C_\omega} \frac{\partial k}{\partial x_j} \frac{\partial \omega}{\partial x_j} \tag{35}$$

In order to retrieve a positive Yap-correction when transformed back to the ε-equation it is necessary to have $C_\omega < (1/\sigma_\omega + 1/\sigma_k)$. In the present model it is numerically optimised as, $C_\omega = 1.1$, which yields a positive Yap-correction in the near-wall region with $C_\varepsilon = -0.45$.

For comparison, Table 1 lists C_ω and C_ε for relevant models, where C_ω and C_ε are the model constants for the turbulent cross-diffusion in the ω-equation (Eq. (35)) and ε-equation (Eq. (33)), respectively.

2.4.4. Model constants

The model constants of a $k - \omega$ model may be obtained from the transformation of a $k - \varepsilon$ model as in Eq. (19) which suggests that $C_{\omega 1} = C_{\varepsilon 1} - 1$ and $C_{\omega 2} = C_k(C_{\varepsilon 2} - 1)$. For the present model the value of $C_{\omega 2}$ is

Table 1
Turbulent cross-diffusion coefficients, from various turbulence models

Model	C_ω	σ_k	$\sigma_\varepsilon, \sigma_\omega$	C_ε
Menter (1994)	1.712	1	1.17	−0.143
Yoon and Chung (1995)	1.07	1	0.75	−1.26
Peng et al. (1997)	0.75	0.8	1.35	−1.25
Wilcox (1998)	0.3	1	1.67	−1.3
Rahman and Siikonen (2000)	0.77	1	1.3	−1
Kok (2000)	0.5	1.5	2	−0.67
Present	1.1	1	1.8	−0.45

set to 0.072, using analogy to decaying turbulence, Eq. (32). In the standard $k - \varepsilon$ model $C_{\varepsilon 1} = 1.44$, (Launder and Spalding, 1974) here a slightly tweaked value, 1.49, is applied, which translates to $C_{\omega 1} = 0.49$.

The Wilcox $k - \omega$ models (1988, 1993) uses rather high turbulent Schmidt numbers of $\sigma_k = 2$ and $\sigma_\omega = 2$. One of the reasons for this is probably due to the neglected cross-diffusion terms, as compared with a transformed ε-equation. The addition of these terms to the present model ensure that the standard value for the $k - \varepsilon$ model of $\sigma_k = 1$ can be applied. The value for σ_ω is connected to $C_{\omega 1}$ and $C_{\omega 2}$ through the log-law

$$C_{\omega 1} = \frac{C_{\omega 2}}{C_k} - \frac{\kappa^2}{\sqrt{C_k C_\mu} \sigma_\omega} \qquad (36)$$

With $\kappa = 0.41$, the appropriate value for the turbulent Schmidt number is, $\sigma_\omega = 1.8$.

2.5. The new $k - \omega$ turbulence model

In summary the new $k - \omega$ turbulence model has been developed in the following forms:

$$\frac{Dk}{Dt} = P_k - C_k k \omega + \frac{\partial}{\partial x_j}\left[\left(v + \frac{v_t}{\sigma_k}\right)\frac{\partial k}{\partial x_j}\right]$$

$$\frac{D\omega}{Dt} = C_{\omega 1}\frac{\omega}{k}P_k - C_{\omega 2}\omega^2 + C_\omega\left(\frac{v}{k} + \frac{v_t}{k}\right)\frac{\partial k}{\partial x_j}\frac{\partial \omega}{\partial x_j}$$
$$+ \frac{\partial}{\partial x_j}\left[\left(v + \frac{v_t}{\sigma_\omega}\right)\frac{\partial \omega}{\partial x_j}\right]$$

The turbulent viscosity is given by

$$v_t = C_\mu f_\mu \frac{k}{\omega}$$

$$f_\mu = 0.09 + \left(0.91 + \frac{1}{R_t^3}\right)\left[1 - \exp\left\{-\left(\frac{R_t}{25}\right)^{2.75}\right\}\right]$$

with the turbulent Reynolds number defined as $R_t = k/(\omega v)$. The constants in the model are given as

$$C_k = 0.09, \quad C_\mu = 1, \quad C_\omega = 1.1, \quad C_{\omega 1} = 0.49,$$
$$C_{\omega 2} = 0.072, \quad \sigma_k = 1, \quad \sigma_\omega = 1.8$$

3. Solution procedure

3.1. Numerical method

The new model was implemented and evaluated using the incompressible finite-volume method code CALC-BFC (Davidson and Farhanieh, 1995). The code employs the second-order bounded differencing scheme (van Leer, 1974) for the convective derivates, and the second-order central differencing scheme for the other terms. The SIMPLE-C algorithm was used to deal with the velocity–pressure coupling. CALC-BFC uses boundary-fitted-coordinate, on a non-staggered grid with the Rhie–Chow (1983) interpolation to smooth non-physical oscillations. In order to improve the diagonal domination in the TDMA solver, the cross-diffusion terms are added to the left-hand side if they are negative and on the right-hand side otherwise.

3.2. Boundary conditions

For the BFS flow, all variables are prescribed in the inlet, while the Neumann condition are used at the outlet. For the channel flow and rib-roughened cases, periodic boundary conditions are applied for the inlet and outlet boundaries. On the walls, no-slip condition is used, $U_i = 0$, $k = 0$. The boundary condition for ω is set using the asymptotic relation, Eq. (21), for the first two nodes to ensure the correct derivate at the wall. Following Wilcox (1998), this asymptotic relation is valid only for $y^+ < 2.5$ and hence it is of importance to refine the mesh to ensure that at least the first two nodes stay within this limit. Wilcox suggest that 7–10 grid points are needed to eliminate any numerical errors. However, it has been shown previously (Bredberg, 1999) that this requirement can be relaxed substantially with little effect on the predicted results, even for near-wall critical properties such as the Nusselt number.

4. Results and discussion

The new $k - \omega$ turbulence model is evaluated and compared with other turbulence models for three different test-cases: the fully developed turbulent channel flow, $Re_\tau = 395$ (Moser et al., 1999), the BFS flow, $Re_h = 5100$ (Le et al., 1997), and a rib-roughened channel, $Re_H = 30\,000$ (Rau et al., 1998). Previous reviews of turbulence models by e.g. Patel et al. (1985) and Wilcox (1993) concluded that many of the older models are not adequate. The turbulence models used for comparisons are the Wilcox $k - \omega$ (1993) denoted Wilcox, the $k - \varepsilon$ of Abe et al. (1994) (AKN), and a variant of the Durbin $k - \varepsilon - v^2 - f$ model, Lien and Kalitzin (2001), (Durbin).

4.1. Fully developed channel flow

The new $k - \omega$ turbulence model is first validated through a fully developed turbulent channel flow, with $Re_\tau = 395$, (Kim, unpublished work, also Moser et al. (1999)). The test-case is attractive, since periodic inlet–outlet conditions can be applied. The self-similarity also makes 1D computation possible reducing the CPU cost to a minimum. In spite of the simplicity of this test-case, the important wall effects are present in the flow. The channel flow thus represents an appropriate test for

LRN models. In addition, since the case is well analysed in DNS, the model behaviour may be scrutinised to a level not reachable for other test-cases.

Figs. 2 and 3 show the distribution of normalised streamwise velocity and turbulent kinetic energy, respectively, in comparison with DNS data. Included in the figures are also the predicted results from the models by Lien and Kalitzin (2001), Abe et al. (1994) and Wilcox (1993).

The present model yields predictions in excellent agreement with the DNS data. The Wilcox model generally underpredicts the velocity profile while the Durbin model overestimates the velocity. The peak in the turbulent kinetic energy is predicted as $k^+ = 4.3$, by the present model, similar to the Wilcox and Durbin model, while the AKN model underestimate k. DNS data gives $k^+ = 4.57$. The predicted result for the turbulent shear stress and dissipation rate, ε, (not shown here), is similar to other two-equation models.

4.2. Backward-facing step

For the BFS flow, the flow undergoes separation, recirculation and re-attachment followed by a re-developing boundary layer. In addition, this flow involves a shear-layer mixing process, as well as an adverse pressure, thus the BFS is an attractive flow for calibrating turbulence models.

The case used here is the one that has been studied using DNS by Le et al. (1997). This case has a relatively low Reynolds number, $Re_h = 5100$, based on the step-height, h. In the present computation the inflow condition is specified using DNS data at $x/h = -10$. Neumann condition is applied for all variables at the outlet located at $x/h = 30$. No-slip condition is used on
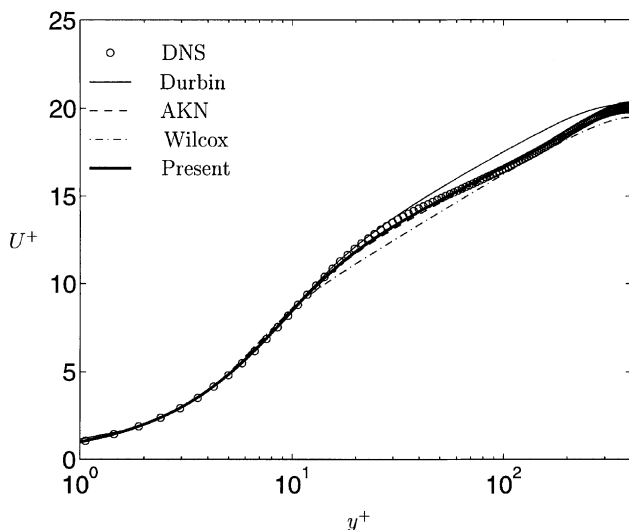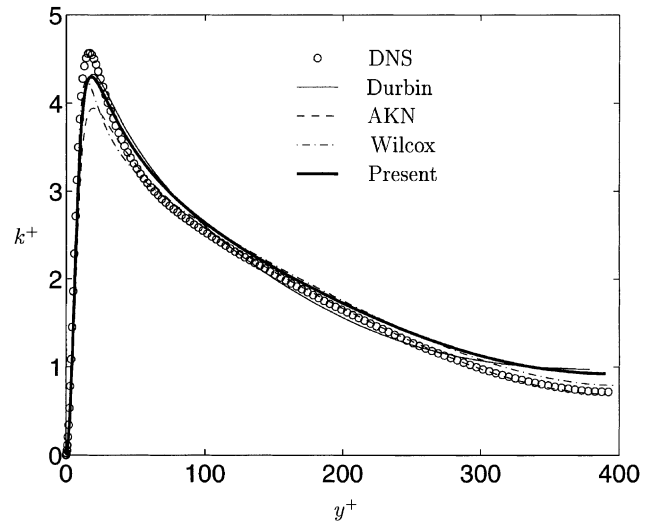

Fig. 3. Turbulent kinetic energy, channel flow at $Re_\tau = 395$.

the walls. The overall calculation domain ranges from $x/h = -10$ to 30, with the step located at $x/h = 0$. The channel height is $5h$ in the inlet section and $6h$ after the step, yielding an expansion ratio of 1.2. A grid-dependency study was performed with two different meshes; a coarse mesh with 100×90 nodes and, a fine mesh with 200×180 nodes. Both meshes gives almost identical predictions although a discrepancy of about 1% is caused in the predicted re-attachment length, through the usage of the coarse mesh. It should be noted that the re-attachment length is a parameter most sensitive to the grid refinement.

The inlet condition in the BFS-case is crucial for a critical evaluation and comparison. The DNS data of Spalart (1988) for the velocity profile and the k-profile, are directly applied at the inlet. The inflow ε or ω is specified in such a way that the model prediction matches the DNS data at $x/h = -3$.

The skin friction coefficient, defined as: $C_f = 2\tau_w / (\rho U_\infty^2)$, is shown in Fig. 4. One of the commonly used quantities to justify the accuracy of a turbulence model in a BFS-case is the re-attachment length of the main separation. The present model gives, $x_r/h = 6.3$, which is close to that of the DNS data, $x_r/h = 6.28$. The other models give; $x_r/h = 7.6$ (Durbin), $x_r/h = 5.7$ (AKN) and $x_r/h = 7.8$ (Wilcox). The skin friction coefficient is well predicted but with some discrepancies in the re-developing region ($x/h > 10$), where the present model predicts a too rapid recovery to turbulent flow, notable in Fig. 4, through the overestimation of C_f. This process is highly effected by the diffusion of turbulent kinetic energy, hence the value of σ_k. For the present model, C_f can be slightly improved by increasing σ_k, however with a degraded representation of the velocity profile as a consequence.

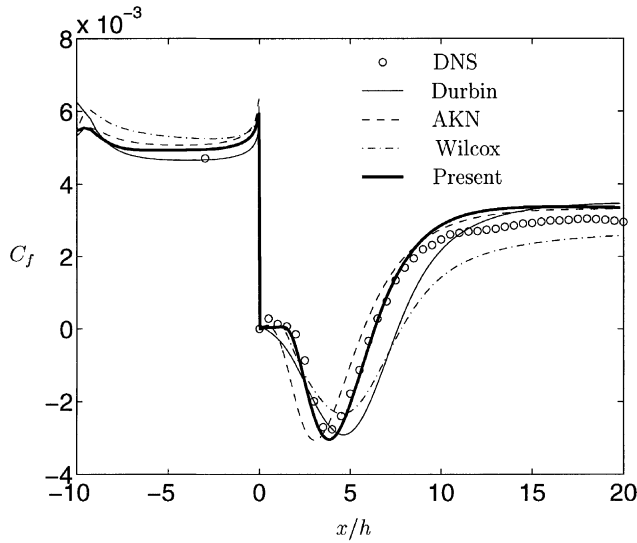Fig. 2. Velocity profile, channel flow at $Re_\tau = 395$.
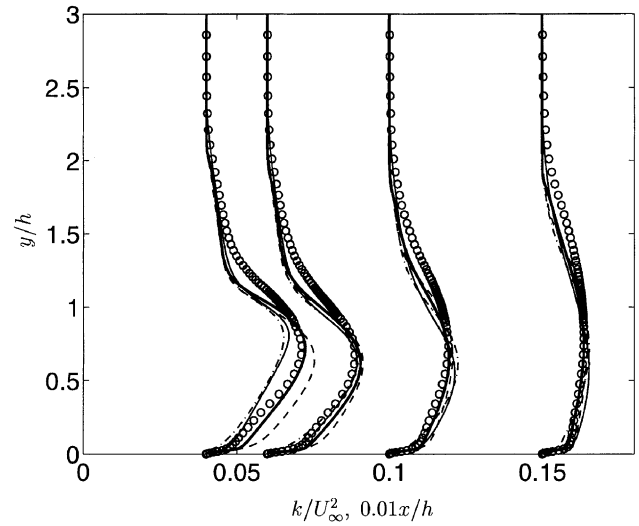
Fig. 4. Skin friction coefficient, BFS-case.

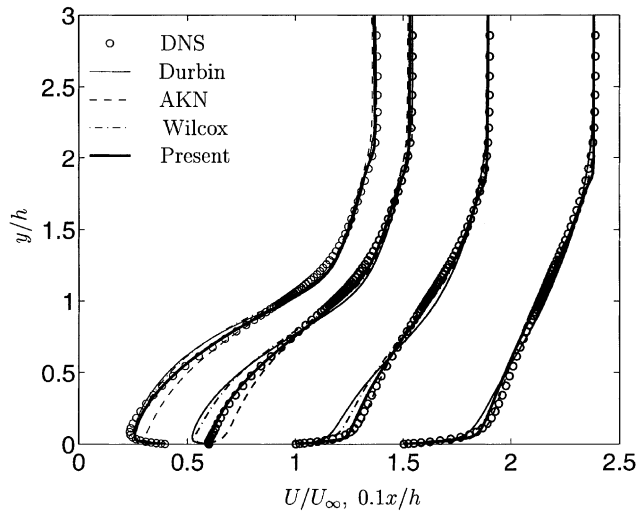Fig. 6. Normalised turbulent kinetic energy at $x/h = 4, 6, 10$ and 15, BFS-case. Legend as in Fig. 5.

Fig. 5. Normalised mean velocity at $x/h = 4, 6, 10$ and 15, BFS-case.

The normalised streamwise velocity profiles, U/U_∞ at $x/h = 4, 6, 10$ and 15 are shown in Fig. 5. The profiles matches the DNS data perfectly at $x/h = -3$ for all models (not shown), which was a pre-request for the prescribed inlet conditions. In the re-circulation zone, $0 \leqslant x/h \leqslant 6$ the present model, gives markedly improved predictions as compared with the other models, particular near the region of the re-attachment point (i.e. at $x/h = 6$). In the re-developing zone, $x/h \geqslant 10$ the present model recovers quickly and matches the DNS data fairly accurate.

The normalised turbulent kinetic energy profiles, k/U_∞^2 are shown in Fig. 6. In the re-circulation zone, at $x/h = 4$ and 6, the predicted turbulent kinetic energy is connected to the predicted size of the bubble. A low turbulence level (Durbin and Wilcox models) gives a large bubble, while the opposite is valid for the AKN-

model. All models underpredict the turbulence level in the mixing shear-layer, $y/h \approx 1.5$, similar to what Peng and Davidson (2000) found in their predictions of the same case.

The accuracy of the predicted turbulent kinetic energy with the present model is overall better than the other models. Note that in the outer region of the boundary layer, all the models used underestimate the turbulence level. The level of reduction is connected to the value of σ_k, and the magnitude of the turbulent cross-diffusion. Increasing C_ω for the cross-diffusion term, and/or σ_k results in a more pronounced reduction of the turbulence level at the edge of the boundary layer. The present model represents an acceptable combination of the two constants. It should be noted that the cross-diffusion term acts as production terms in this region, increasing ω, and hence reducing the eddy-viscosity. A benefit from this construction, as noted by Menter (1991) is that the model becomes less sensitive to the freestream value of ω, which otherwise is a drawback of the standard $k - \omega$ model (see Fig. 1).

The profiles of the normalised shear stress, $\overline{uv}/U_\infty^2$, are shown in Fig. 7. The connection between the turbulence level and the size of the re-circulation zone is even more accentuated in these figures, where the Durbin and Wilcox models severely underpredict the shear stress at $x/h = 4$ and 6. Beyond the re-attachment point the results are improved for $y/h < 1$, while the results in the shearing layer, $y/h \approx 1.5$ are generally underpredicted.

4.3. Rib-roughened channel

The heat transfer performance of the present model is evaluated in the rib-roughened case (RR) of Rau et al.
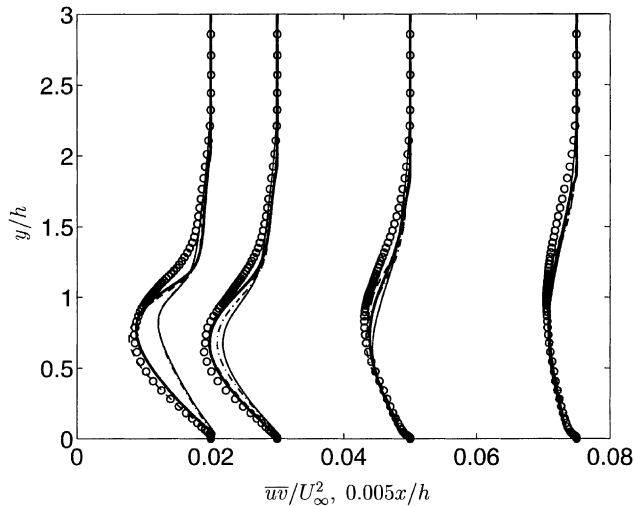
Fig. 7. Normalised shear stress at $x/h = 4$, 6, 10 and 15, BFS-case. Legend as in Fig. 5.

Fig. 8. Grid dependency, RR-case

(1998). The Reynolds number, based on the mean velocity and the hydraulic diameter, D_h, is $Re_D = 30\,000$. In the experiment, constant heat flux boundary condition was supplied through resisting heating, with the wall temperature pattern provided by liquid crystals. The channel, measuring $50 \times 50 \times 1000$ mm, was made of Plexiglas, to provide visual observation. The ribs, which were insulated, and of size: 5×5 mm, giving a ratio of height-to-channel hydraulic diameter, e/D_h, of 0.1. Different locations of the ribs were used in the experiment, here only the pitch-to-height ratio, P/e, of 9 with single-sided ribs case is used for comparison. The experiment provides both flow field and heat transfer measurements. In the present study the centreline streamwise velocity and Nusselt number are used in the comparison. The measured Nusselt numbers were normalised with the Dittus–Boelter equation (Dittus and Boelter, 1930) as introduced by McAdams (1942)

$$Nu_\infty = 0.023 Re^{0.8} Pr^{0.4} \qquad (37)$$

The uncertainty in the resulting enhancement factor, Nu/Nu_∞, was estimated to be 5% for the experiment.

The computations were made using periodic boundary condition at the streamwise boundaries, which was verified in the experiment to prevail in the test section. This reduces the uncertainty in the result due to the inlet boundary condition. No-slip condition and constant heat flux were applied at the walls. The rib was, as in the experiment, insulated. In the present computation a 2D mesh with: 100×120 nodes was used. A grid-independent study is shown in Fig. 8, where the mesh refinement was reduced to half and doubled, respectively. As seen, the computation on different meshes gives only a marginal effect on the predicted Nusselt number. The result on the 100×120, mesh is considered asymptotically valid.
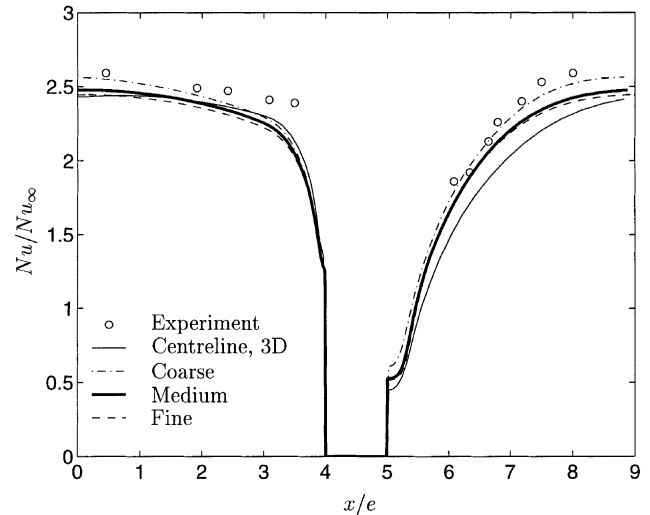
A 2D simulation for a channel with aspect ratio of one may be questioned, due to the side-wall effects. The side-wall induced secondary flows modify the centreline streamwise velocity, however, whereas the local heat transfer in the centre of the duct is only marginally affected, which was also noted by Ooi et al. (2000). The slight difference in predicted Nusselt number can be observed in Fig. 8, where a comparison is made between a 3D mesh ($50 \times 60 \times 25$) and three 2D meshes (coarse: 50×60, used: 100×120 and fine: 200×240). Based on these results, it was felt confident to use the results from the 2D computations for the discussion. In addition, a comparison between the present results with the predictions by Ooi et al. (1998) confirms the accuracy of the numerical method.

The predicted streamwise velocity and turbulent viscosity are compared with the experimental data in Fig. 9. The velocity profiles are normalised using the bulk velocity, $U_b = \dot{m}/(A\rho)$. Since no vertical profiles of a turbulent quantity, were presented in Rau et al. (1998), the profiles of the turbulent viscosity are included only as complementary data, and to aid in understanding the behaviour of the models. The predicted turbulent viscosity is normalised using the kinematic viscosity, ν. The computation domain measures $x/e = 9$ by $y/e = 10$, with the rib located in the centre of the domain from $x/e = 4$ to 5. The profiles are shown only from the lower wall to the centreline, with their origin located at $x/e = 4.5$ (centred on the rib) and $x/e = 8.5$. The latter location is close to the measured re-attachment point of $9.0 < x_r/e < 9.25$.

The present model predicts overall an accurate distribution of the streamwise velocity, compared to the measured data. The AKN model predicts, as for the BFS-case, too a short re-circulation bubble, while the Wilcox and Durbin model yield too a long bubble. None
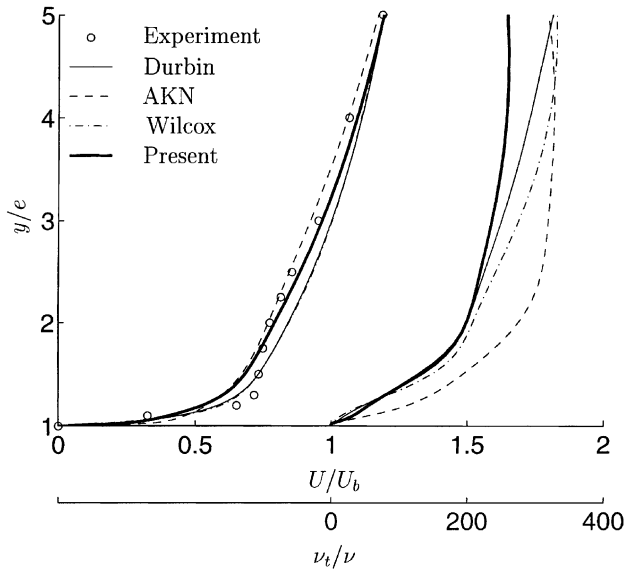
(a) $x/e = 4.5$ (rib-top)
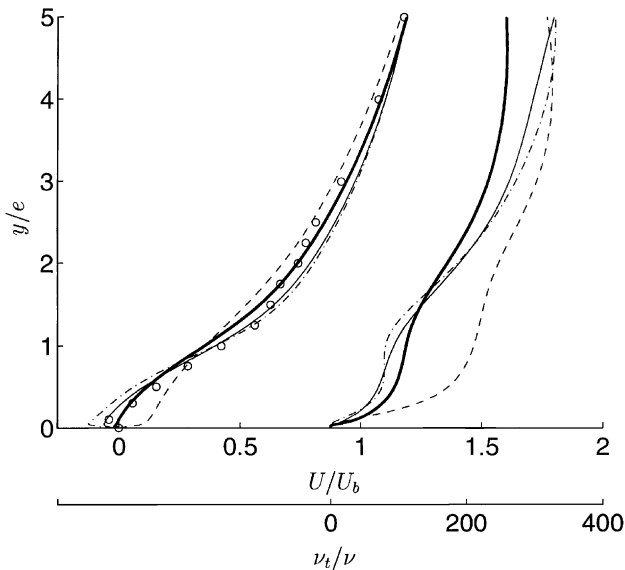
(b) $x/e = 8.5$ (re-attachment)

Fig. 9. Velocity and turbulent viscosity, RR-case.

Fig. 10. Nusselt number, RR-case.

of the models reproduces accurately the sharp velocity gradient on the rib, or the intensive backflow in the re-circulation zone. As noted from the turbulent viscosity profiles, the velocity profiles are closely connected to the predicted level of turbulent viscosity. In general, the AKN model yields a high level of turbulence while the Wilcox model gives a low one.

Two different approaches are used to specify the turbulent Prandtl number, Pr_t in the present prediction: either a constant Prandtl number according to Eq. (7), or an algebraic relation as proposed by Kays and Crawford, Eq. (8). A comparison betw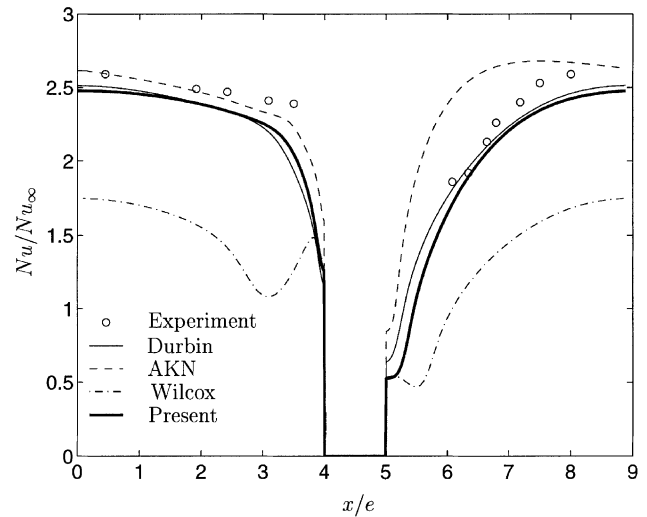een the Kays–Crawford formulation and the constant turbulent Prandtl number, with $Pr_t = 0.9$ yields only a marginal difference in the predicted heat transfer. A decrease of the turbulent Prandtl number to $Pr_t = 0.8$, resulted in a general increase in the Nusselt number by 5%. For the presented results the Kays and Crawford heat transfer model was used.

Fig. 10 compares the Nusselt numbers predicted from the different turbulence models. Both the present model and the Durbin model give reasonable predictions, while the Wilcox model underpredicts the Nusselt number, and the AKN yields discrepancies immediately downstream the rib.

In a previous work (Bredberg et al., 2000), for a similar rib-roughened configuration, a discussion was made on the close connection between heat transfer and turbulence level. It is re-confirmed in this computation. The AKN-model which predicts a high level of turbulence also overestimates the heat transfer, while the Wilcox model underestimates the heat transfer as a result of the low levels of ν_t. This is consistently reflected in the BFS-case where the re-attachment length was underestimated by the AKN model and overpredicted by the Wilcox model.

In contrast the Durbin model reproduces rather an accurate heat transfer, in spite of its underestimation of turbulence, Fig. 9(b). The reason may be attributed to the formulation of the eddy-viscosity, in the Durbin model, which contrary to the standard EVMs, is based on two velocity scales, the turbulent kinetic energy, k, and the wall normal fluctuating velocity $\overline{vv}$.

5. Conclusions

In this study an improved $k - \omega$ turbulence model is presented. The model is evaluated through comparison

with available DNS and experiment data and with three EVMs. The present model yields improved results for all test-cases compared with the original Wilcox $k - \omega$ model. The model gives similar or improved predictions as compared with the numerically and computational more demanding four-equation $k - \varepsilon - v^2 - f$ model of Durbin.

The present model includes both viscous and turbulent cross-diffusion terms, in the ω-equation. Using an analogy to the Yap-correction, through TSDIA, the turbulent cross-diffusion is theoretically founded, and its importance to reduce the sensitivity to the freestream value of ω is demonstrated. The viscous cross-diffusion term represent an model for the pressure-diffusion process, and also enables the present model to use the DNS consistent boundary condition for the specific dissipation rate, $\omega_w = 2v/C_k y^2$. Using the improved modelling the number of empirical damping functions could be reduce to one.

Acknowledgements

References

Abe, K., Kondoh, T., Nagano, Y., 1994. A new turbulence model for predicting fluid flow and heat transfer in separating and reattaching flows—I. flow field calculations.. Int. J. Heat Mass Trans. 37, 139–151.

Bredberg, J., 1999. Prediction of flow and heat transfer inside turbine blades using EARSM, $k - \epsilon$ and $k - \omega$ turbulence models. Thesis for the Degree of Licentiate of Engineering. Department of Thermo and Fluid Dynamics, Chalmers University of Technology, Gothenburg. Available from <www.tfd.chalmers.se/~bredberg>.

Bredberg, J., Davidson, L., Iacovides, H., 2000. Comparison of near-wall behavior and its effect on heat transfer for $k - \omega$ and $k - \epsilon$ turbulence models in rib-roughened 2D channels. In: Nagano, Y., Hanjalic, K., Tsuji, T. (Eds.), 3rd International Symposium on Turbulence Heat and Mass Transfer, Aichi Shuppan.

Davidson, L., Farhanieh, B., 1995. CALC-BFC. Report 95/11. Department of Thermo and Fluid Dynamics Chalmers, University of Technology, Gothenburg.

Dittus, F., Boelter, L., 1930. Heat transfer in automobile radiators of the tubular type. Univ. Calif. Pubs. Eng. 2, 443–461.

Hanjalic, K., Launder, B., 1976. Contribution towards a Reynolds-stress closure for low-Reynolds-number turbulence. J. Fluid Mech. 74, 593–610.

Huang, P., Bradshaw, P., 1995. Law of the wall for turbulent flows in pressure gradients. AIAA J. 33, 624–632.

Hwang, C., Lin, C., 1998. Improved low-Reynolds-number $k - \epsilon$ model based on direct numerical simulation data. AIAA J. 36, 38–43.

Jones, W., Launder, B., 1972. The prediction of laminarization with a two-equation model of turbulence. Int. J. Heat Mass Trans. 15, 301–314.

Kawamura, H., 1991. A $k - \epsilon - \overline{v^2}$ model with special relevance to the near wall turbulence. In: 8th Symposium on Turbulent Shear Flows.

Kays, W., Crawford, M., 1993. Convective Heat and Mass Transfer. McGraw-Hill Inc, New York.

Kok, J., 2000. Resolving the dependence on freestream values for the $k - \omega$ turbulence model. AIAA J. 38, 1292–1295.

Launder, B., Sharma, B., 1974. Application of the energy-dissipation model of turbulence to the calculation of flow near a spinning disc. Lett. Heat Mass Trans. 1, 131–138.

Launder, B., Spalding, D., 1974. The numerical computation of turbulent flows. Comput. Meth. App. Mech. Eng. 3, 269–289.

Le, H., Moin, P., Kim, J., 1997. Direct numerical simulation of turbulent flow over a backward-facing step. J. Fluid Mech. 330, 349–374.

Lien, F., Kalitzin, G., 2001. Computations of transonic flow with the $v^2 - f$ turbulence model. Int. J. Heat Fluid Flow 22, 53–61.

Mansour, N., Kim, J., Moin, P., 1988. Reynolds-stress and dissipation-rate budgets in a turbulent channel flow. J. Fluid Mech. 194, 15–44.

McAdams, W., 1942. Heat Transmission, second ed. McGraw-Hill, New York.

Menter, F., 1991. Influence of freestream values on $k - \omega$ turbulence model predictions. AIAA J. 30, 1657–1659.

Menter, F., 1994. Two-equation eddy-viscosity turbulence models for engineering applications. AIAA J. 32, 1598–1605.

Moser, R., Kim, J., Mansour, N., 1999. Direct numerical simulation of turbulent channel flow up to $Re = 590$. Phys. Fluids 11, 943–945. Available from <www.tam.uiuc.edu/Faculty/Moser/>.

Ooi, A., Iaccarino, G., Behnia, M., 1998. Heat transfer predictions in cavaties. In: Centre for Turbulence Research Summer Program 1998.

Ooi, A., Reif, B.P., Iaccarino, G., Durbin, P., 2000. Evaluation of RANS for rotating flows. In: Centre for Turbulence Research Summer Program 2000.

Patel, V., Rodi, W., Scheuerer, G., 1985. Turbulence models for near-wall and low Reynolds number flows: a review. AIAA J. 23, 1308–1319.

Peng, S.-H., Davidson, L., 2000. New two-equation eddy viscosity transport model for turbulent flow computation. AIAA J. 38, 1196–1205.

Peng, S.-H., Davidson, L., Holmberg, S., 1997. A modified low-Reynolds-number $k - \omega$ model for recirculating flows. J. Fluid Eng. 119, 867–875.

Rahman, M., Siikonen, T., 2000. Improved low-Reynolds-number $k - \epsilon$ model. AIAA J. 38, 1298–1300.

Rau, G., Cakan, M., Moeller, D., Arts, T., 1998. The effect of periodic ribs on the local aerodynamic and heat transfer performance of a straight cooling channel. J. Turbomach. 120, 368–375.

Rhie, C., Chow, W., 1983. Numerical study of the turbulent flow past an airfoil with trailing edge separation. AIAA J. 21, 1525–1532.

Rodi, W., Mansour, N., 1993. Low Reynolds number $k - \epsilon$ modelling with the aid of direct numerical simulation. J. Fluid Mech. 250, 509–529.

Spalart, P., 1988. Direct simulation of a turbulent boundary layer up to $R_\theta = 1410$. J. Fluid Mech. 187, 61–98.

Speziale, C., Abid, R., Anderson, E., 1992. Critical evaluation of two-equation models for near-wall turbulence. AIAA J. 30, 324–331.

Townsend, A., 1976. The Structure of Turbulent Shear Flow. Cambridge University Press, Cambridge.

van Leer, B., 1974. Towards the ultimate conservative difference monotonicity and conservation combined in a second-order scheme. J. Comput. Phys. 14, 361–370.

Wilcox, D., 1988. Reassessment of the scale-determining equation for advanced turbulence models. AIAA J. 26, 1299–1310.

Wilcox, D., 1993. Comparison of two-equation turbulence models for boundary ayers with pressure gradient. AIAA J. 31, 1414–1421.

Wilcox, D., 1998. Turbulence Modeling for CFD. DCW Industries Inc.

Yap, C., 1987. Turbulent heat and momentum transfer in recirculation and impinging flows. Ph.D. thesis, Department of Mechanical Engineering, Faculty of Technology, University of Manchester.

Yoon, B., Chung, M., 1995. Computation of compression ramp flow with a cross-diffusion modified $k - \epsilon$ model. AIAA J. 33, 1518–1520.

Yoshizawa, A., 1987. Statistical modeling of a transport equation for the kinetic energy dissipation rate. Phys. Fluids 30, 628–631.